Available online at website: https://journal.bcrec.id/index.php/bcrec

Bulletin of Chemical Reaction Engineering & Catalysis, 20 (2) 2025, 381-391

Original Research Article

Impact of Zirconia and Lanthanum Promoters on Multiwalled CNT Generation in Dry Reforming of Methane

Wan Nabilah Manan[1], Wan Nor Roslam Wan Isahak[1,2,*], Zahira Yaakob[1,*], Salma Samidin[1]

[1]Department of Chemical and Process Engineering, Faculty of Engineering and Built Environment, Universiti Kebangsaan Malaysia, 43600 UKM Bangi, Selangor, Malaysia
[2]Research Center for Sustainable Process Technology (CESPRO), Faculty of Engineering and Built Environment, Universiti Kebangsaan Malaysia, 43600 UKM Bangi, Selangor, Malaysia

Received: 30th December 2024; Revised: 7th May 2025; Accepted: 8th May 2025
Available online: 10th May 2025; Published regularly: August 2025

Abstract

In this study, three distinct carbon nanotubes (CNTs) — Zr-Ni/CeO_2, La-Ni/CeO_2, and Ni/CeO_2 were produced via dry reforming of methane (DRM) at 800°C for 180 minutes. These catalysts were initially synthesized using ultrasonic-assisted citric impregnation method to enhance metal promoter dispersion. X-ray diffraction (XRD) confirmed that Zr and La doping minimized carbon deposition. Brunauer-Emmett-Teller (BET) analysis revealed typical mesoporous structures of stacked laminar nanorods. Thermogravimetric analysis (TGA) quantified carbon deposits as Zr-Ni/CeO_2 (5.1 wt%) < La-Ni/CeO_2 (7.85 wt%) < Ni/CeO_2 (11.3 wt%). TEM and FESEM confirmed the formation of multiwalled carbon nanotubes (MWCNTs), while XPS provided insights into surface chemistry, oxidation states, and defect sites. Doping with Zr and La enhanced crystallinity, CeZr phase formation, thermal stability, and reduced carbon deposition, with MWCNTs exhibiting higher graphitization (I_G/I_D: Zr-Ni/CeO_2 = 1.25, La-Ni/CeO_2 = 1.59) compared to Ni/CeO_2 (I_G/I_D = 1.15). This discovery represents a breakthrough in catalyst development, providing a dual advantage of reducing carbon deposition and boosting H_2 production in the Dry Reforming of Methane (DRM) process. The carbon formed is primarily multi-walled carbon nanotubes (MWCNTs), which not only minimize harmful carbon accumulation but also enhance overall catalytic performance. This innovation offers a sustainable solution for carbon management and the conversion of greenhouse gases.

Keywords: carbon nanotubes; dry reforming of methane; ceria; zirconia; lanthanum

How to Cite: Manan, W. N., Wan Isahak, W. N. R., Yaakob, Z., Samidin, S. (2025). Impact of Zirconia and Lanthanum Promoters on Multiwalled CNT Generation in Dry Reforming of Methane *Bulletin of Chemical Reaction Engineering & Catalysis*, 20 (2), 381-391. (doi: 10.9767/bcrec.20266)

Permalink/DOI: https://doi.org/10.9767/bcrec.20266

1. Introduction

The pressing concerns of global warming and the finite availability of petroleum-based energy resources have spurred the need for sustainable alternatives to conventional energy sources [1]. Renewable energy, such as solar power, biomass, and biogas, has gained significant attention as a viable path toward a greener future [2,3]. Catalytic processes that facilitate the efficient conversion of these renewable resources into valuable products have become a key focus of research. Among these processes, dry reforming of methane (DRM) stands out due to its dual role in utilizing biogas while simultaneously reducing greenhouse gas emissions by converting methane (CH_4) and carbon dioxide (CO_2) into syngas, a valuable precursor for fuels and chemicals [4]. DRM chemical reaction:

$$CH_4\,(g) + CO_2\,(g) \rightleftharpoons 2CO\,(g) + 2H_2\,(g), \quad \Delta H^{\circ}_{298\ K} = +247\ kJ/mol \qquad (1)$$

* Corresponding Author.
Email: wannorroslam@ukm.edu.my (W.N.R Wan Isahak)

In recent years, CeO_2-based catalysts have emerged as a promising solution for the DRM reaction due to their excellent redox properties, oxygen storage capacity, and strong metal-support interactions. The Ce^{4+}/Ce^{3+} cycle facilitates oxygen transfer, helping to oxidize carbon deposits and maintain catalyst stability [5]. Additionally, CeO_2 enhances metal dispersion, improves thermal stability, and promotes CO_2 activation through its moderate surface basicity, making it an ideal support for efficient and durable DRM catalyst.

Building on the advantages of CeO_2, further performance improvements can be achieved by strategic doping with suitable promoters. Among various promoters, zirconium (Zr) and lanthanum (La) have attracted considerable attention due to their ability to enhance the physicochemical properties of CeO_2-supported Ni catalysts. Zr incorporation improves the oxygen mobility and creates additional oxygen vacancies, which enhance carbon oxidation and prevent coke accumulation [6,7]. Meanwhile, La increases the surface basicity of CeO_2, promoting CO_2 adsorption and activation, which is crucial for carbon removal during DRM [8]. The combined modifications aim to improve catalyst stability, metal dispersion, and resistance to carbon deposition, addressing key challenges typically encountered in DRM systems.

The primary challenge in large-scale dry reforming lies in establishing a catalyst system that is both highly active and exceptionally stable. The material must resist coke formation and prevent sintering at operating temperatures [9]. The accumulation of coke easily coats the metal particles, clogging the catalyst pores and causing substantial deactivation of the catalyst [9,10]. Various forms of coke, such as amorphous and filamentous carbon, accumulate on the surface of Ni-based catalysts during hydrocarbon reforming. It is widely recognized that these carbon deposits generally have negative impacts on the catalyzed reaction [11,12]. Nevertheless, there is evidence indicating that the development of specific carbon types on the Ni surface can indeed yield favourable outcomes [13,14].

Carbon nanotubes (CNTs) possess distinctive characteristics, including large surface areas, mesoporous structures, a uniform distribution of pore sizes, and resistance to elevated temperatures as well as acidic or alkaline environments [15]. As shown in Figure 1, there are two types of carbon nanotubes, i.e. single walled carbon nanotubes (SWCNT) and multi walled carbon nanotubes (MWCNT). Both have promising applications in bioscience and nanotechnology due to their high purity, tunable dimensions, surface functional groups, and unique electronic properties. [16].The uniqueness of nanotubes arises from their structure, featuring a helically arranged pattern of carbon atoms in hexagonal arrays on their surface honeycomb lattices [17].

The structure of carbon nanotubes, whether single-walled or multi-walled, depends not only on the catalyst composition but also on the preparation method used [19]. The utilization of bimetallic catalysts has revealed synergistic catalytic effects in the production of carbon nanotubes from hydrocarbons. The CNT growth is notably influenced by the composition of the bimetallic catalyst [19]. He *et al*. [20] demonstrated that Carbon Nanotubes (CNTs) formation positively impacts catalyst conversion and stability during reforming.

In this study, Ni/CeO_2 catalysts doped with zirconium (Zr) and lanthanum (La) were developed to enhance catalytic performance and promote carbon nanotube (CNT) formation during dry reforming of methane. The catalysts were synthesized using a modified impregnation technique to improve metal dispersion. This work aims to evaluate the effect of Zr and La doping on the type of carbon formed, including its crystallinity, morphology, graphitization degree, and extent of carbon deposition.

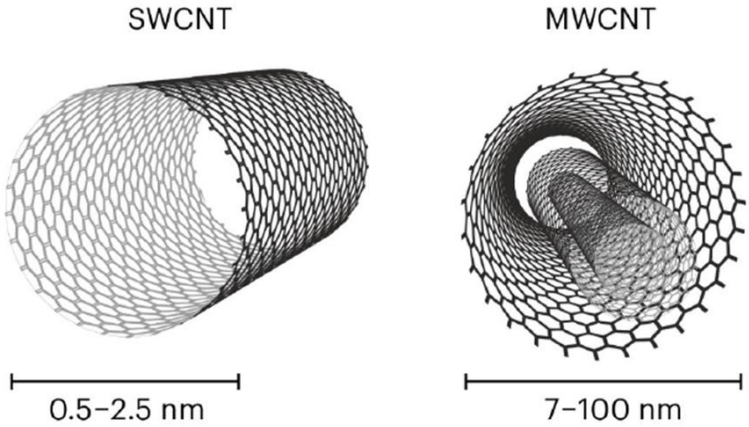

Figure 1. Images of SWCNT and MWCNT [18]

2. Materials and Methods

2.1 Catalyst Synthesis

2.1.1 Preparation of Ni/CeO_2 catalyst

The Ni/CeO_2 catalyst was prepared using ultrasonic-assisted citrate impregnation. $Ni(NO_3)_2.6H_2O$ and $Ce(NO_3)_3.6H_2O$ (both 99%, Sigma-Aldrich) were dissolved in deionized water and heated to 40 °C with continuous stirring [21]. In a separate solution, citric acid ($C_6H_8O_7H_2O$) was dissolved in deionized water and slowly added to the salt mixture, followed by stirring for 1 hour at 40 °C. The combined solution was then placed in an ultrasonic bath and heated to 60 °C until most of the water evaporated, which took about 3 hours, forming a light green solid. This solid was dried at 110 °C for 24 hours and then calcined at 550 °C for 4 hours with a heating rate of 10 °C per minute. The resulting Ni/CeO_2 catalyst was ground into a fine powder.

2.1.2 Synthesis of $x/NiCeO_2$ (x=Zr, La)

A specified amount of metal promoters (2 wt% Zr and 2 wt% La) was added separately to the Ni/CeO_2 solution in different beakers, and the mixtures were heated to 40 °C with continuous stirring. Afterward, they were transferred to an ultrasonic bath and heated to 60 °C until most of the water evaporated. The resulting mixtures were then dried at 110 °C for 24 hours, followed by calcination at 550 °C for 4 hours to form a uniform nano-oxide blend and eliminate impurities. The final catalysts were labelled Ni/CeO_2, $Zr\text{-}Ni/CeO_2$, and $La\text{-}Ni/CeO_2$. The catalysts were tested under DRM conditions at 800 °C for 180 minutes, and the resulting CNTs were thoroughly characterized to assess their structure, surface properties, and catalytic efficiency.

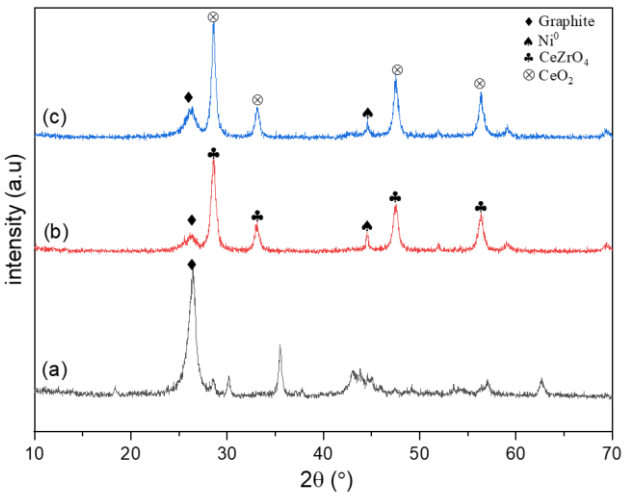

Figure 2. XRD diffractogram for spent catalyst (a) Ni/CeO_2, (b) $Zr\text{-}Ni/CeO_2$, (c) $La\text{-}Ni/CeO_2$

2.2 Characterization of Catalysts

X-ray diffraction (XRD) was performed using a Bruker D8 Advance diffractometer, operating at 40 kV and 40 mA, with Ni-filtered Cu-Kα radiation (λ = 0.15406 nm). The diffraction patterns were recorded over a 2θ range of 5–80° at a scanning rate of 0.25° s^{-1}, and average crystallite size was calculated using Scherrer's equation. Nitrogen adsorption-desorption isotherms were obtained at −196 °C using a Micromeritics Tristar II Plus 3030KR, with surface areas and pore structures determined by BET and BJH methods. Transmission electron microscopy (TEM) analysis was conducted with an FEI Talos L120C at 120 kV. X-ray photoelectron spectroscopy (XPS) was performed using a Kratos Axis Ultra DLD with Al-Kα radiation (1486 eV), with the C 1s signal at 284.5 eV used for peak calibration. Raman spectra were acquired using a laser excitation line at 514.5 nm. Thermogravimetric analysis of carbon deposits was performed using DSC 214 Polyma equipment.

3. Results and Discussion

3.1 XRD Characterization results

Figure 2 shows the XRD diffraction patterns of carbon species formed on spent catalysts after the DRM reaction. The peak at 2θ ≈ 26.6° corresponds to the graphitic carbon [002] plane, while the peak at 2θ ≈ 44.5° represents the [100] plane of metallic Ni associated with graphitic carbon formation [22]. Among the samples, $Zr\text{-}Ni/CeO_2$ exhibited the lowest intensity and a slight shift in the [002] peak position, indicating reduced carbon deposition and a more disordered carbon structure. In contrast, the undoped Ni/CeO_2 showed the highest peak intensity, confirming greater carbon accumulation. The reduced carbon signal for the Zr-doped catalyst is attributed to the formation of a $CeZrO_x$ solid solution, which enhances oxygen mobility and facilitates the oxidation of carbon species, thereby suppressing carbon buildup [23]. Similarly, La doping improved performance by increasing surface basicity, which promotes CO_2 adsorption and gasification of carbon intermediates. The overall trend in graphitic carbon deposition follows the order of Ni/CeO_2 > $La\text{-}Ni/CeO_2$ > $Zr\text{-}Ni/CeO_2$—clearly demonstrates that Zr and La doping effectively minimizes carbon accumulation, thus improving catalyst stability. Additionally, the presence of the CeZr mixed oxide phase (PDF 00-067-0078) contributes to redox cycling [24], accelerating coke gasification and lowering total carbon deposition to as low as 5.1 wt% at 800 °C. This structural and redox synergy is essential for maintaining long-term activity in DRM and promoting controlled CNT formation.

3.2 Surface Properties and Pore Characteristics Analysis

Figure 3(a) shows the N_2 adsorption-desorption isotherms of the spent catalysts, all of which exhibit type IV isotherms with H3-type hysteresis loops at high relative pressures (P/Po = 0.85–0.99), indicating mesoporous structures typically associated with aggregated plate-like particles or lamellar CNT morphologies [25]. Among the samples, the undoped Ni/CeO_2 catalyst demonstrates the smallest hysteresis loop and the lowest adsorption volume, suggesting a lower surface area and fewer mesopores, which likely limits gas diffusion and active site accessibility during DRM [26]. In contrast, both Zr- and La-doped Ni/CeO_2 catalysts display significantly higher adsorption volumes and larger hysteresis loops [27], confirming enhanced mesoporosity and surface area due to better CNT formation and structural modification by the dopants.

As shown in Figure 3(b), the pore size distribution further supports these findings. The La-Ni/CeO_2 catalyst presents a bimodal distribution with prominent mesopores at 4–5 nm (internal pores) and additional mesopores between 15–30 nm, attributed to interstitial voids formed between multi-walled CNTs. Zr-Ni/CeO_2 also shows an extended mesopore range, facilitating greater capillary condensation and gas adsorption. The improved porosity and surface area in the doped catalysts enhance the diffusion of CH_4 and CO_2, promote uniform CNT growth, and contribute to better catalytic performance by increasing the number of accessible active sites and improving coke management [28,29].

Table 1 proves that the CNT with doping with promoters (Zr and La) exhibit higher surface area and smaller pore structures than CNT without doping (CNT Ni/CeO_2). For carbon nanotubes (CNTs) in hydrogen storage, higher surface area and smaller pores are typically advantageous. A larger surface area offers more sites for hydrogen adsorption, boosting storage capacity, while smaller pores help confine hydrogen molecules, enhancing their interaction with the nanotube surface [30]. However, finding a balance is crucial,

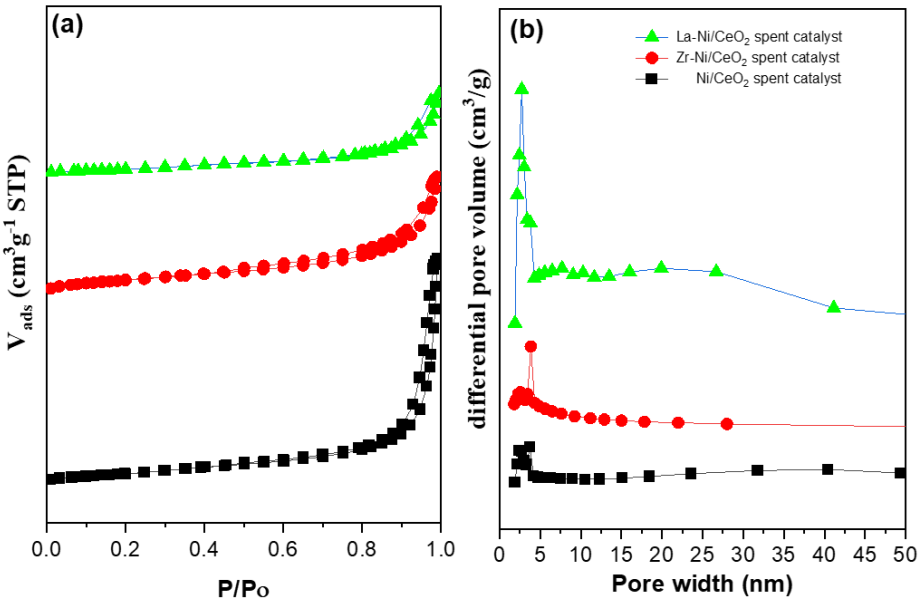

Figure 3. (a) N_2 adsorption isotherm curves (b) Pore size distribution for the used/post-reaction Ni/CeO_2, Zr-Ni/CeO_2 and La-Ni/CeO_2 catalyst series.

Table 1. (a) N_2 adsorption isotherm curves (b) Pore size distribution for the used/post-reaction Ni/CeO_2, Zr-Ni/CeO_2 and La-Ni/CeO_2 catalyst series ([a] obtained via Brunauer-Emmett-Teller (BET) equation; [b] BJH; [c] value obtained using the Scherer equation)

Catalysts	BET-BJH Method			XRD
	Surface Area ($m^2.g^{-1}$)[a]	Total Pore Volume ($cm^3.g^{-1}$)[b]	Average Pore Diameter (nm) [b]	Crystallite size of NiO (111) (nm)[c]
CNT $NiCeO_2$	55.1	0.299	19.2	8.52
CNT $Zr/NiCeO_2$	63.2	0.163	9.4	8.65
CNT $La/NiCeO_2$	59.3	0.174	14.0	9.40

as very small pores may limit hydrogen diffusion, impacting adsorption and desorption rates. The ideal pore size and structure depend on the specific application for hydrogen storage.

3.3 Raman Analysis

Figure 4 presents the Raman spectra of the spent catalysts, showing three main peaks: the D band (~1340 cm^{-1}) associated with disordered carbon, the G band (~1590 cm^{-1}) linked to graphitic sp^2 carbon, and the 2D band (~2675 cm^{-1}), indicative of graphitic layer stacking and CNT quality [31]. The intensity ratio (I^G/I^D) reflects the degree of graphitization [32], with higher values indicating better structural order and fewer defects. The I^G/I^D ratios for Ni/CeO_2, Zr-Ni/CeO_2, and La-Ni/CeO_2 were 1.15, 1.25, and 1.59, respectively. These results demonstrate that La doping yields the highest graphitic quality, followed by Zr, both outperforming the undoped catalyst. The enhanced graphitization in the doped catalysts suggests more controlled CNT formation and fewer amorphous carbon deposits, contributing to improved catalytic stability and resistance to deactivation. This supports the role of Zr and La in tuning the carbon structure and promoting the growth of high-quality CNTs during DRM.

3.4 TGA Analysis

Thermogravimetric analysis (TGA) was used to quantify carbon deposition on the spent catalysts after the DRM reaction. As shown in Figure 5, mass loss above 400 °C corresponds to carbon oxidation [33]. The total carbon content followed the trend: Ni/CeO_2 (11.3 wt%) > La-Ni/CeO_2 (7.85 wt%) > Zr-Ni/CeO_2 (5.1 wt%). The significantly lower carbon residue in the doped catalysts indicates enhanced resistance to carbon accumulation. This improvement is attributed to increased surface basicity [34] and oxygen mobility introduced by La and Zr dopants, which promote CO_2 activation [27] and generate active oxygen species capable of gasifying carbon intermediates. These findings confirm that Zr and La doping enhances the catalyst's ability to suppress coke formation, thus improving long-term stability and catalytic performance in DRM. Table 2 summarises the result of TGA and Raman spectra analysis.

3.5 EDX Mapping Characterization

Figure 6 and Figure 7 show the EDX analysis of the spent $NiCeO_2$ catalyst samples with different metal promoters. The EDX quantification analysis confirmed the TGA analysis's result that the carbon formation is reduced with the addition of Zr and La promoters. Significant heterogeneity in Ce distribution within individual particles was found to influence carbon morphology. For instance, particles with an average Ce composition of approximately 50 at. % generated long CNTs rather than short ones [19].

3.6 FESEM Morphology Characterization

Figure 8 shows the FESEM images of the spent Zr-Ni/CeO_2 (a, c) and La-Ni/CeO_2 (b, d) catalysts after the DRM reaction, revealing the

Table 2. Summary of TGA and Raman Analysis results.

Catalysts	Amount of carbon deposits (%)	Intensity ratio of G/D
Ni/CeO_2	11.31%	1.15
Zr-Ni/CeO_2	5.1%	1.25
La-Ni/CeO_2	7.85%	1.59

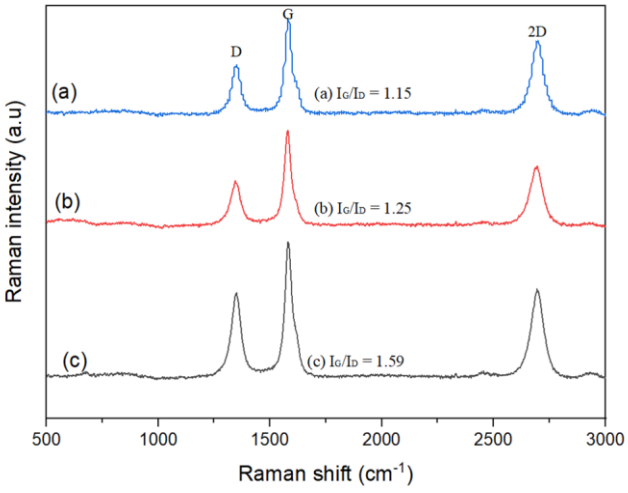

Figure 4. Raman spectrum of the nanocarbon deposited on (a) Ni/CeO_2, (b) Zr-Ni/CeO_2, and (c) La-Ni/CeO_2.

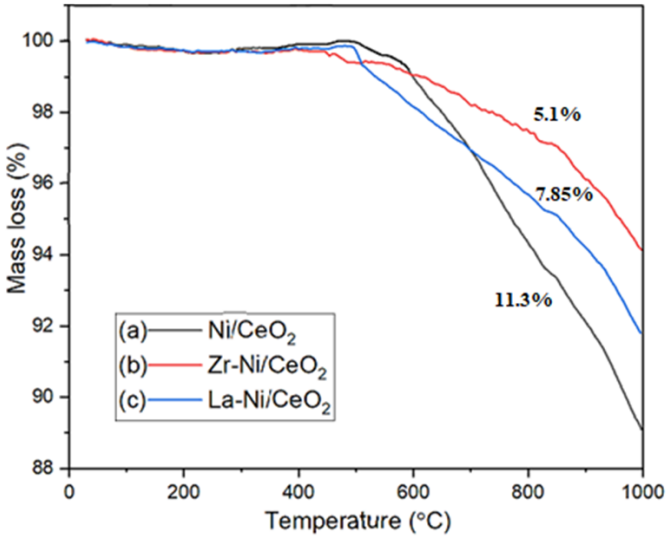

Figure 5. TGA analysis for spent catalysts.

formation of fibrous and coiled carbon structures typical of filamentous carbon or multi-walled carbon nanotubes (MWCNTs). This type of carbon grows outward from the catalyst surface and is less likely to block active sites [35], thus minimizing catalyst deactivation. The presence of Zr and La promotes the formation of well-structured filamentous carbon, rather than amorphous carbon, due to their roles in enhancing metal dispersion, oxygen mobility, and surface basicity [36]. These features not only suppress excessive carbon accumulation but also allow stable CNT growth, maintaining catalytic activity and improving the longevity of the catalyst in DRM.

3.7 TEM Morphology Characterization

TEM analysis revealed the formation of multi-walled carbon nanotubes (MWCNTs) in all spent catalysts, with the Zr-Ni/CeO_2 (Figure 9b, 9e) sample displaying the most uniform and well-defined structures. The Zr-Ni/CeO_2 catalyst displays thin-walled, well-aligned carbon nanotubes with uniform metal dispersion and minimal aggregation, indicating reduced sintering and sustained catalytic activity—

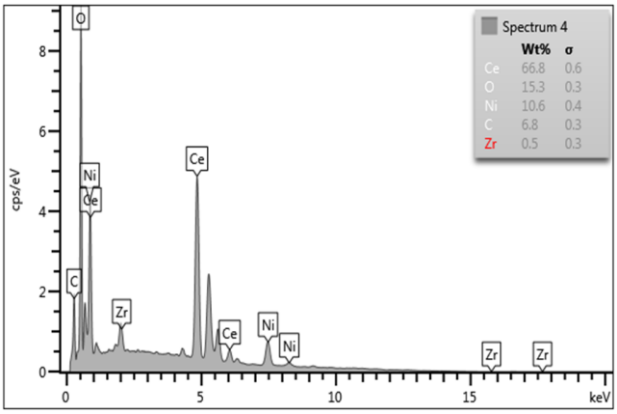

Figure 6. EDX mapping for Zr-Ni/CeO_2 spent catalyst.

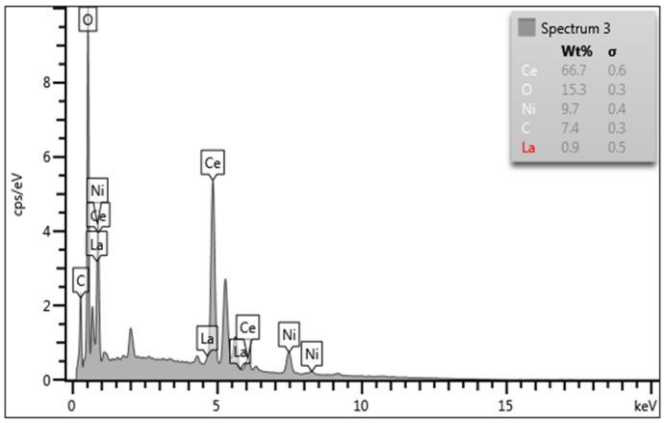

Figure 7. EDX mapping for La-Ni/CeO_2 spent catalyst.

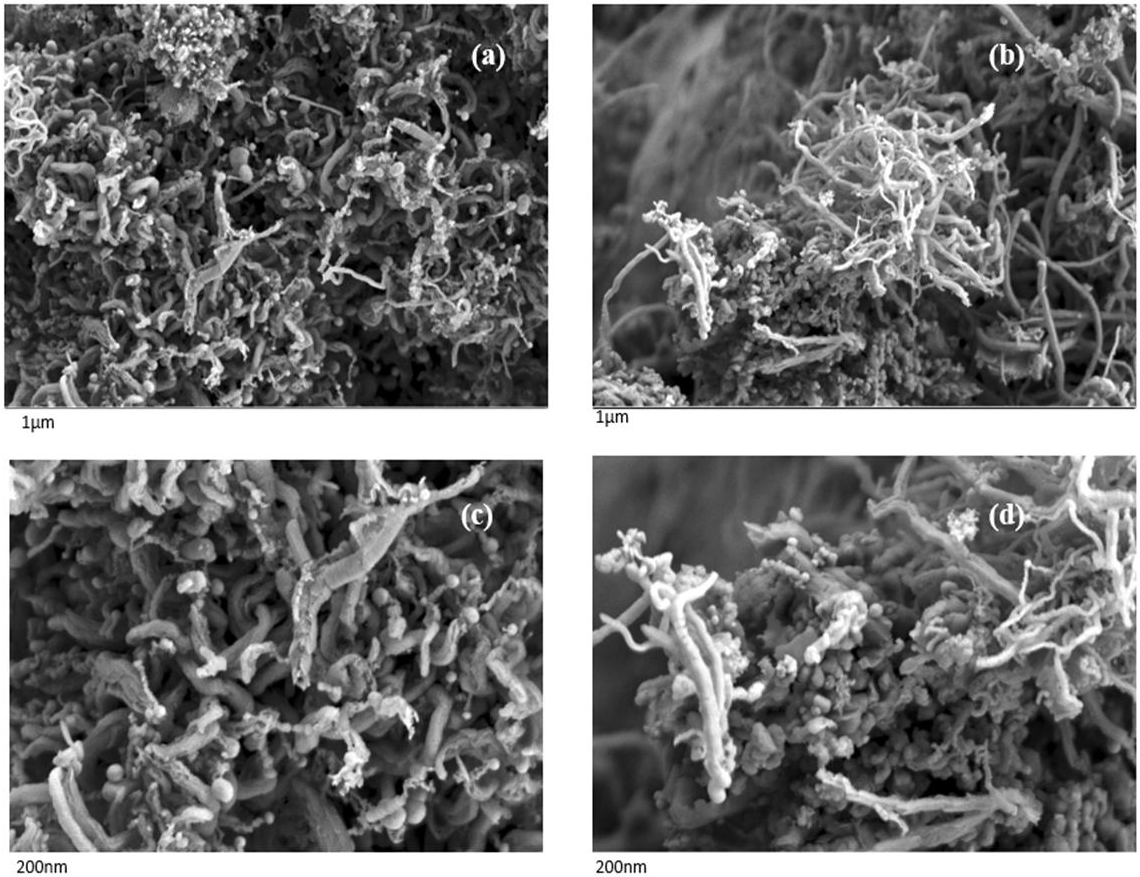

Figure 8. FESEM morphology for spent catalyst (a&c) Zr-Ni/CeO_2 and (b&d) La-Ni/CeO_2.

consistent with findings by [37] which report that thin-walled CNTs exhibit higher reactivity due to a greater proportion of surface atoms.

The formation of structured MWCNTs, especially in the Zr-doped catalyst, stabilizes metal particles, reduces sintering, and preserves active surface area. Additionally, the CNT morphology can influence reaction kinetics and support sustained catalytic activity [20], highlighting the role of Zr and La in enhancing both CNT quality and catalyst durability during DRM.

The TEM images indicated the presence of filamentous carbon in the samples, allowing for the measurement of both internal and external diameters. For the spent Zr-Ni/CeO_2 catalyst (Figure 9e), the internal diameter was found to be 20.44 nm, while the external diameter measured 34.79 nm, with a spacing of 6.5 nm. In contrast, the spent Ni/CeO_2 (Figure 9d) and La-Ni/CeO_2 (Figure 9f) catalysts exhibited smaller internal diameters, ranging from 9.58 nm to 10.97 nm. These filamentous carbon structures are classified as multi-walled carbon nanotubes (MWCNTs), which typically have diameters between 10 and 40 nm [38]. The formation of MCNTs can help stabilize the catalyst by providing a protective carbon layer around the active metal sites. This stabilization can prevent sintering and loss of active surface area, allowing the catalyst to maintain its activity for hydrogen production over extended periods [37]. MWCNTs can facilitate alternative reaction pathways by stabilizing reaction products via Van der Waals interactions and affecting the kinetics of competing reactions, with their diameter playing a key role in this process [39].

3.8 Surface Chemical Properties Analysis

This XPS analysis was performed using both wide scan and narrow scan for the carbon samples formed on the catalysts after the reaction. Based on the wide scan in Figure 10, the elements detected on the spent catalyst Zr-Ni/CeO_2 are only O1s and C1s. XPS analysis was performed to examine the surface chemical characteristics of carbon formed on the Zr-Ni/CeO_2 catalyst during DRM. In the C1s spectrum (Figure 11a), the peak at 284.5 eV corresponds to graphitic carbon, indicating stable carbon structures that do not deactivate the catalyst. The peak at 286.2 eV reflects carbon-oxygen functionalities (C=O, C-O, -COOH), [42] suggesting surface oxidation that may enhance H_2 production and the H_2/CO ratio [43]. The peak at 282.05 eV indicates carbon-metal (C–Ni) bonding, which is critical for methane decomposition at active sites [44]. In the O1s spectrum (Figure 11b), the peak at 530.2 eV is attributed to lattice oxygen in CeO_2 [45], which facilitates redox activity and carbon removal. Peaks at 531.9 eV and 533.1 eV correspond to surface hydroxyl groups and adsorbed water [44],

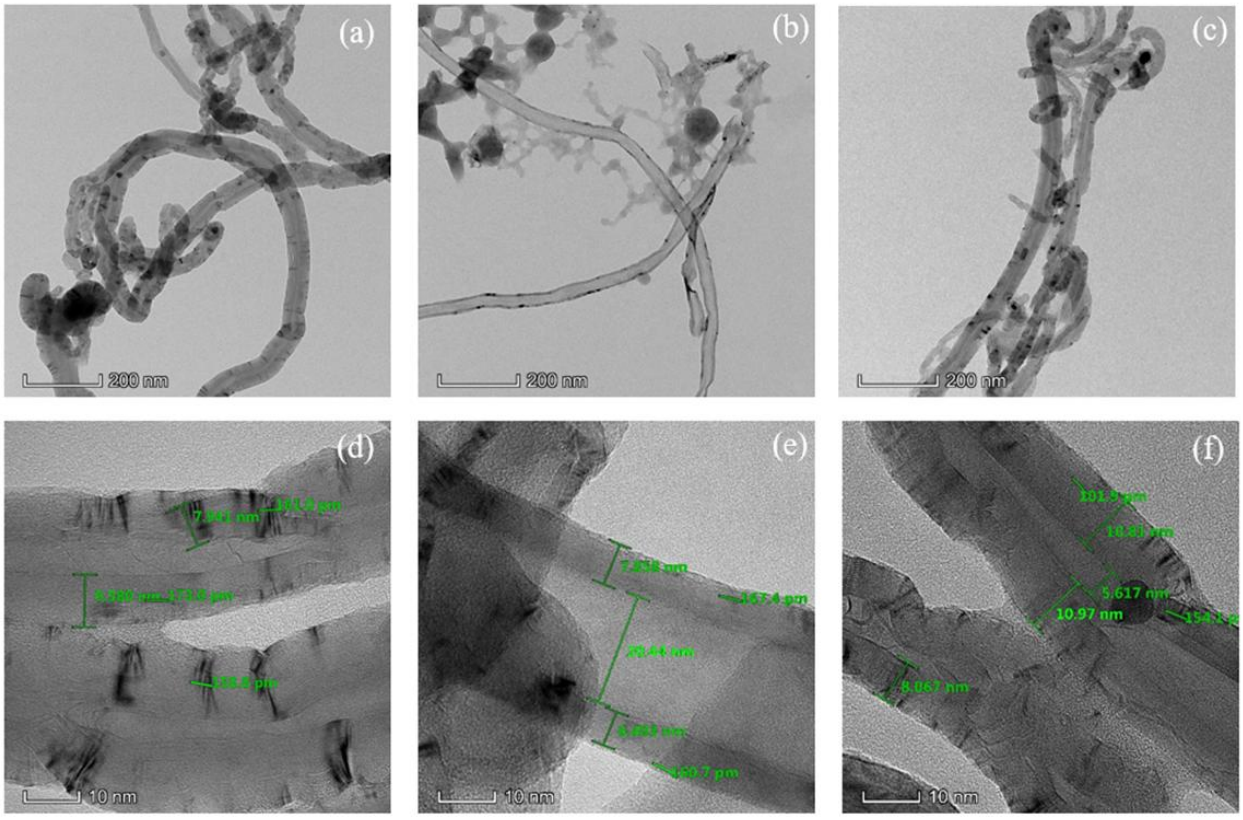

Figure 9. TEM image for used catalyst (a,d) Ni/CeO_2, (b,e) Zr-Ni/CeO_2, (c,f) La-Ni/CeO_2.

which also participate in the DRM mechanism. Overall, the XPS results confirm that the Zr-Ni/CeO_2 catalyst exhibits favorable surface chemistry, including graphitic carbon, metal-carbon bonding, and active oxygen species, that supports enhanced catalytic performance in DRM.

The occurrence of multi-walled carbon nanotubes (MWCNTs) in the Zr-Ni/CeO_2 and La-Ni/CeO_2 spent catalyst enhances hydrogen (H_2) production while reducing the formation of poisonous carbon deposits. MWCNTs provide a large surface area and active sites that improve catalytic efficiency, allowing more effective adsorption and decomposition of hydrocarbons. Table 3 shows the carbon deposits from this study compared to previous research findings.

Table 3. Comparison of the findings of this study with previous researchers' studies.

Catalysts	Reaction Conditions	Carbon deposited (wt %)	Refs.
5Ni/CeO_2	T:800 °C, R:CH_4:CO_2	62.7	[46]
$NiCe_{0.1}Zr_{0.9}O_3$	T:800 °C, R:CH_4:CO_2	10.7	[47]
Ni@CeO_2	T:800 °C, R:CH_4:CO_2	1.6 rate of carbon	[48]
Ni@$CeZrO_2$ Ni/$CeZrO_2$ (75 bt% CeO_2)	T:700 ◦C, R:CH_4:CO_2	3.5	[49]
Zr-Ni/CeO_2 La-Ni/CeO_2 Ni/CeO_2	T:800 °C, R:3CH_4:2CO_2	5.1 7.85 11.31	This research

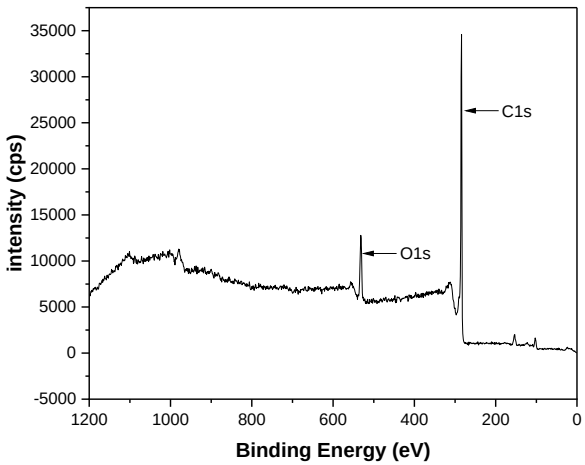

Figure 10. Wide scan XPS spectrum of the spent catalyst Zr-Ni/CeO_2.

4. Conclusion

CeO_2-based catalysts demonstrate strong potential for dry reforming of methane (DRM), enabling simultaneous conversion of greenhouse gases and production of valuable carbon nanotubes (CNTs). Spent Ni/CeO_2, Zr-Ni/CeO_2, and La-Ni/CeO_2 catalysts generated well-structured multi-walled CNTs, highlighting their dual role in catalysis and nanomaterial synthesis. Zr and La doping enhanced CNT formation by improving surface area, porosity, and graphitization, as confirmed by XRD, BET, and Raman analyses. TGA showed significantly reduced carbon deposition in doped catalysts, while FESEM and TEM revealed uniform CNT morphology and minimal particle aggregation, especially in Zr-doped samples. These synergistic enhancements improve catalyst stability and performance, positioning Zr- and La-modified Ni/CeO_2 as promising materials for efficient carbon utilization and sustainable energy applications.

Acknowledgement

This work was supported by the Fundamental Research Grant Scheme (FRGS) grant funded by the Ministry of Higher Education of Malaysia, project code: FRGS/1/2019/TK02/UKM/01/2 and industry project code: KK-2020-013. The authors

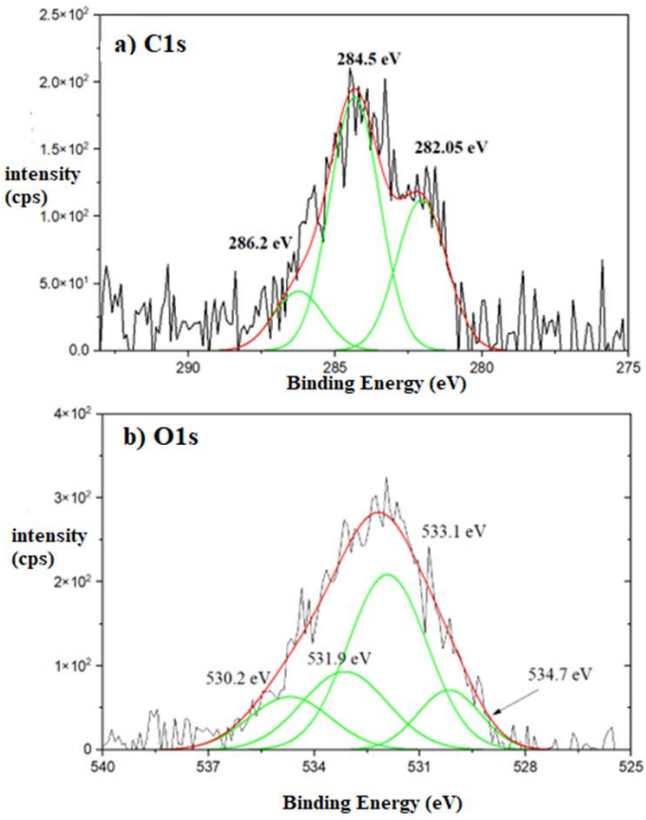

Figure 11. Narrow scan XPS spectrum of (a) C1s and (b) O1s peaks for the Zr-Ni/CeO_2 spent catalyst.

would also like to thank the i-CRIM Laboratory, ALAF-UKM, for analytical services.

CRediT Author Statement

Author Contributions: Conceptualization, W.N.M and S.S.; validation, W.N.R.W.I and Z.Y.; investigation, W.N.M.; resources, W.N.R.W.I.; data curation, W.N.M and S.S.; writing; W.N.M supervision, W.N.R.W.I and Z.Y.; funding acquisition, W.N.R.W.I. All authors have read and agreed to the published version of the manuscript.

References

[1] Salehi, S., Alavi, S.M., Rezaei, M., Akbari, E., Varbar, M. (2024) Syngas production from dry reforming of glycerol by the NiO/M-Al2O3 catalysts: Effect of various support promoters and various ZrO2 content. *J. CO2 Util.* 81, 102737. DOI: 10.1016/j.jcou.2024.102737.

[2] Kludpantanapan, T., Rattanaamonkulchai, R., Srifa, A., Koo-Amornpattana, W., Chaiwat, W., Sakdaronnarong, C., Charinpanitkul, T., Assabumrungrat, S., Wongsakulphasatch, S., Aieamsam-Aung, P., et al. (2022) Development of CoMo-X catalysts for production of H2 and CNTs from biogas by integrative process. *J. Environ. Chem. Eng.* 10, 107901. DOI: 10.1016/j.jece.2022.107901.

[3] Bahari, N.A., Wan Isahak, W.N.R., Masdar, M.S., Yaakob, Z. (2019) Clean hydrogen generation and storage strategies via CO2 utilization into chemicals and fuels: A review. *Int. J. Energy Res.* 43, 5128–5150. DOI: 10.1002/er.4498.

[4] Maziviero, F.V., Melo, D.M.A., Medeiros, R.L.B.A., Silva, J.C.A., Araújo, T.R., Oliveira, Â.A.S., Silva, Y.K.R.O., Melo, M.A.F. (2024) Influence of Mn, Mg, Ce and P promoters on Ni-X/Al2O3 catalysts for dry reforming of methane. *J. Energy Inst.* 113. DOI: 10.1016/j.joei.2024.101523.

[5] Manan, W.N., Wan Isahak, W.N.R., Yaakob, Z. (2022) CeO2-Based Heterogeneous Catalysts in Dry Reforming Methane and Steam Reforming Methane: A Short Review. *Catalysts,* 12. DOI: 10.3390/catal12050452.

[6] Lanre, M.S., Al-fatesh, A.S., Fakeeha, A.H., Kasim, S.O., Ibrahim, A.A., Al-Awadi, A.S., Al-Zahrani, A.A., Abasaeed, A.E., Ayodele, B.V., Khan, M.R., et al. (2022) Catalytic performance of lanthanum promoted Ni/ZrO2 for carbon dioxide reforming of methane. *Catalysts*, 41, 3899–3912. DOI: 10.1021/acs.iecr.9b02434.

[7] Bespalko, Y., Smal, E., Simonov, M., Valeev, K., Fedorova, V., Krieger, T., Cherepanova, S., Ishchenko, A., Rogov, V., Sadykov, V. (2020) Novel ni/ce(ti)zro2catalysts for methane dry reforming prepared in supercritical alcohol media. *Energies*, 13. DOI: 10.3390/en13133365.

[8] Greluk, M., Rotko, M., Turczyniak-Surdacka, S. (2020) Enhanced catalytic performance of La2O3 promoted Co/CeO2 and Ni/CeO2 catalysts for effective hydrogen production by ethanol steam reforming: La2O3 promoted Co(Ni)/CeO2 catalysts in SRE. *Renew. Energy*, 155, 378–395. DOI: 10.1016/j.renene.2020.03.117.

[9] Muraza, O., Galadima, A. (2015) A review on coke management during dry reforming of methane. *Int. J. Energy Res.* 39, 1196–1216. DOI: 10.1002/er3295.

[10] Mallikarjun, G., Sagar, T.V., Swapna, S., Raju, N., Chandrashekar, P., Lingaiah, N. (2020) Hydrogen rich syngas production by bi-reforming of methane with CO2over Ni supported on CeO2-SrO mixed oxide catalysts. *Catal. Today*, 356, 597–603. DOI: 10.1016/j.cattod.2020.01.005.

[11] Arora, S., Prasad, R. (2016) An overview on dry reforming of methane: strategies to reduce carbonaceous deactivation of catalysts. *RSC Adv.*, 6, 108668–108688. DOI: 10.1039/c6ra20450c.

[12] Abdullah, N., Ainirazali, N., Chong, C.C., Razak, H.A., Setiabudi, H.D., Jalil, A.A., Vo, D.V.N. (2020) Influence of impregnation assisted methods of Ni/SBA-15 for production of hydrogen via dry reforming of methane. *Int. J. Hydrogen Energy*, 45, 18426–18439. DOI: 10.1016/j.ijhydene.2019.09.089.

[13] Al-Swai, B.M., Osman, N., Alnarabiji, M.S., Adesina, A.A., Abdullah, B. (2019) Syngas Production via Methane Dry Reforming over Ceria-Magnesia Mixed Oxide-Supported Nickel Catalysts. *Ind. Eng. Chem. Res.*, 58, 539–552. DOI: 10.1021/acs.iecr.8b03671.

[14] Al-Timimi, B.A., Yaakob, Z. (2022) Catalysts for the Simultaneous Production of Syngas and Carbon Nanofilaments Via Catalytic Decomposition of Biogas. In (Edited by Maryam Takht Ravanchi) *Natural Gas - New Perspectives and Future Developments,* DOI: 10.5772/intechopen.101320

[15] Ajayan, P.M., Zhou, O.Z. (2001) Applications of Carbon Nanotubes. *Carbon Nanotub.*, 425, 391–425.

[16] Hamouda, H.I., Abdel-Ghafar, H.M., Mahmoud, M.H.H. (2021) Multi-walled carbon nanotubes decorated with silver nanoparticles for antimicrobial applications. *J. Environ. Chem. Eng.*, 9, 105034. DOI: 10.1016/j.jece.2021.105034.

[17] Allaedini, G., Tasirin, S.M., Aminayi, P., Yaakob, Z., Meor Talib, M.Z. (2016) Carbon nanotubes via different catalysts and the important factors that affect their production: A review on catalyst preferences. *Int. J. Nano Dimens.*, 7, 186–200, DOI: 10.7508/ijnd.2016.03.002.

[18] Filchakova, M. (2023) What are multi walled carbon nanotubes? MWCNT production, properties, and applications Available online: https://tuball.com/articles/multi-walled-carbon-nanotubes (accessed on Nov 10, 2023).

[19] Liao, X.Z., Serquis, A., Jia, Q.X., Peterson, D.E., Zhu, Y.T., Xu, H.F. (2003) Effect of catalyst composition on carbon nanotube growth. *Appl. Phys. Lett.*, 82, 2694–2696. DOI: 10.1063/1.1569655.

[20] He, L., Hu, S., Jiang, L., Syed-Hassan, S.S.A., Wang, Y., Xu, K., Su, S., Xiang, J., Xiao, L., Chi, H., et al. (2017) Opposite effects of self-growth amorphous carbon and carbon nanotubes on the reforming of toluene with Ni/A-Al2O3 for hydrogen production. *Int. J. Hydrogen Energy*, 42, 14439–14448. DOI: 10.1016/j.ijhydene.2017.04.230.

[21] Manan, W.N., Roslam, N., Isahak, W., Yaakob, Z., Samidin, S., Ahmad, N., Latif, N. (2024) Exploring enhanced syngas production via the catalytic performance of metal-doped X-Ni/CeO2 (X = Zr, La, Sr) in the dry reforming of methane. *Journal of Chemical Technology & Biotechnology*, 99 (11), 2420-2433. DOI: 10.1002/jctb.7732.

[22] Świrk, K., Rønning, M., Motak, M., Beaunier, P., Da Costa, P., Grzybek, T. (2019) Ce-and Y-modified double-layered hydroxides as catalysts for dry reforming of methane: On the effect of yttrium promotion. *Catalysts*, 9, 56. DOI: 10.3390/catal9010056.

[23] Shanmugam, V., Zapf, R., Neuberg, S., Hessel, V., Kolb, G. (2017) Effect of ceria and zirconia promotors on Ni/SBA-15 catalysts for coking and sintering resistant steam reforming of propylene glycol in microreactors. *Appl. Catal. B Environ.*, 203, 859–869, DOI: 10.1016/j.apcatb.2016.10.075.

[24] Dębek, R., Galvez, M.E., Launay, F., Motak, M., Grzybek, T., Da Costa, P. (2016) Low temperature dry methane reforming over Ce, Zr and CeZr promoted Ni–Mg–Al hydrotalcite-derived catalysts. *International Journal of Hydrogen Energy*, 41(27), 11616-11623. DOI: 10.1016/j.ijhydene.2016.02.074.

[25] Li, X., Liu, X., Hao, J., Li, L., Gao, Y., Gu, Y., Cao, Z., Liu, J. (2022) Strong Metal-Support Interactions of Ni-CeO2 Effectively Improve the Performance of a Molten Hydroxide Direct Carbon Fuel Cell. *ACS Omega*, 7, 24646–24655. DOI: 10.1021/acsomega.2c02479.

[26] Yang, Q.H., Hou, P.X., Cheng, H.M. (2001) Adsorption and capillarity of nitrogen in inside channel of carbon nanotubes. *Chemical Physics Letters*, 345 (1-2), 18–24. DOI: 10.1016/S0009-2614(01)00848-X.

[27] Ou, Z., Ran, J., Qiu, H., Huang, X., Qin, C. (2023) Uncovering the effect of surface basicity on the carbon deposition of Ni/CeO2 catalyst modified by oxides in DRM. *Fuel*, 335, 126994. DOI: 10.1016/j.fuel.2022.126994.

[28] Catalysts, N., Łamacz, A., Jag, P., Stawowy, M. (2020) Dry Reforming of Methane over CNT-Supported. *Catalysts*, 10 (7), 741. DOI: 10.3390/catal10070741.

[29] Abbaslou, R.M., Vosoughi, V., Dalai, A.K. (2017) Comparison of nitrogen adsorption and transmission electron microscopy analyses for structural characterization of carbon nanotubes. *Appl. Surf. Sci.*, 419, 817–825. DOI: 10.1016/j.apsusc.2017.04.253.

[30] Rather, S.U. (2020) Preparation, characterization and hydrogen storage studies of carbon nanotubes and their composites: A review. *Int. J. Hydrogen Energy*, 45, 4653–4672. DOI: 10.1016/j.ijhydene.2019.12.055.

[31] Li, Y.S., Liao, J.L., Wang, S.Y., Chiang, W.H. (2016) Intercalation-assisted longitudinal unzipping of carbon nanotubes for green and scalable synthesis of graphene nanoribbons. *Sci. Rep.*, 6, 1–12. DOI: 10.1038/srep22755.

[32] Pudukudy, M., Yaakob, Z., Akmal, Z.S. (2015) Direct decomposition of methane over SBA-15 supported Ni, Co and Fe based bimetallic catalysts. *Appl. Surf. Sci.*, 330, 418–430. DOI: 10.1016/j.apsusc.2015.01.032.

[33] Sidik, S.M., Triwahyono, S., Jalil, A.A., Aziz, M.A.A., Fatah, N.A.A., Teh, L.P. (2016) Tailoring the properties of electrolyzed Ni/mesostructured silica nanoparticles (MSN) via different Ni-loading methods for CO2 reforming of CH4. *J. CO2 Util.*, 13, 71–80. DOI: 10.1016/j.jcou.2015.12.004.

[34] Smal, E., Bespalko, Y., Arapova, M., Fedorova, V., Valeev, K., Eremeev, N., Sadovskaya, E., Krieger, T., Glazneva, T., Sadykov, V., et al. (2022) Carbon Formation during Methane Dry Reforming over Ni-Containing Ceria-Zirconia Catalysts. *Nanomaterials*, 12, 3676. DOI: 10.3390/nano12203676.

[35] Baharudin, L., Rahmat, N., Othman, N.H., Shah, N., Syed-Hassan, S.S.A. Formation, control, and elimination of carbon on Ni-based catalyst during CO2 and CH4 conversion via dry reforming process: A review. *J. CO2 Util.*, 61, 102050. DOI: 10.1016/j.jcou.2022.102050.

[36] Hussien, A.G.S.. Polychronopoulou, K. (2022) A Review on the Different Aspects and Challenges of the Dry Reforming of Methane (DRM) Reaction. *Nanomaterials*, 12, 3400. DOI: 10.3390/nano12193400.

[37] Pudukudy, M., Yaakob, Z., Takriff, M.S. (2016) Methane decomposition into COx free hydrogen and multiwalled carbon nanotubes over ceria, zirconia and lanthana supported nickel catalysts prepared via a facile solid state citrate fusion method. *Energy Convers. Manag.*, 126, 302–315. DOI: 10.1016/j.enconman.2016.08.006.

[38] Figueira, C.E., Moreira, P.F., Giudici, R., Alves, R.M.B., Schmal, M. (2018) Nanoparticles of Ce, Sr, Co in and out the multi-walled carbon nanotubes applied for dry reforming of methane. *Appl. Catal. A Gen.*, 550, 297–307. DOI: 10.1016/j.apcata.2017.11.019.

[39] Kong, J., Li, R., Wang, F., Chen, P., Liu, H., Liu, G., Lv, W. (2018) Sulfate radical-induced transformation of trimethoprim with CuFe2O4/MWCNTs as a heterogeneous catalyst of peroxymonosulfate: mechanisms and reaction pathways. *RSC Advances*, 8, 24787–24795. DOI: 10.1039/c8ra04103b.

[40] Abdel Karim Aramouni, N., Zeaiter, J., Kwapinski, W., Ahmad, M.N. (2017) Thermodynamic analysis of methane dry reforming: Effect of the catalyst particle size on carbon formation. *Energy Convers. Manag.*, 150, 614–622. DOI: 10.1016/j.enconman.2017.08.056.

[41] Álvarez, A., Borges, M., Corral-Pérez, J.J., Olcina, J.G., Hu, L., Cornu, D., Huang, R., Stoian, D., Urakawa, A. (2017) CO2 Activation over Catalytic Surfaces. *ChemPhysChem*, 18, 3135–3141. DOI: 10.1002/cphc.201700782.

[42] Kumanek, B., Stando, G., Wróbel, P.S., Krzywiecki, M., Janas, D. (2019) Thermoelectric properties of composite films from multi-walled carbon nanotubes and ethyl cellulose doped with heteroatoms. *Synth. Met.*, 257, 116190. DOI: 10.1016/j.synthmet.2019.116190.

[43] Figueira, C.E., Moreira, P.F., Giudici, R., Alves, R.M.B., Schmal, M. (2018) Nanoparticles of Ce, Sr, Co in and out the multi-walled carbon nanotubes applied for dry reforming of methane. *Appl. Catal. A Gen.*, 550, 297–307. DOI: 10.1016/j.apcata.2017.11.019.

[44] Isahak, W.N.R.W., Hasan, S.Z., Ramli, Z.A.C., Ba-Abbad, M.M., Yarmo, M.A. (2018) Enhanced physical and chemical adsorption of carbon dioxide using bimetallic copper–magnesium oxide/carbon nanocomposite. *Res. Chem. Intermed.*, 44, 829–841. DOI: 10.1007/s11164-017-3138-6.

[45] Wei, Y., Song, M., Yu, L., Meng, F. (2021) CO2 reforming of methane over carbon fiber-lanthanum oxide supported bimetallic nickel-cobalt catalysts: Kinetic and mechanistic studies. *Process Saf. Environ. Prot.*, 145, 236–246. DOI: 10.1016/j.psep.2020.08.007.

[46] Taufiq-Yap, Y.H., Sudarno, Rashid, U., Zainal, Z. (2013) CeO2-SiO2 supported nickel catalysts for dry reforming of methane toward syngas production. *Appl. Catal. A Gen.*, 468, 359–369, DOI: 10.1016/j.apcata.2013.09.020.

[47] Yuan, W., Wang, Y., Zou, Y., Tan, W., Hou, W., Zheng, L., Wu, F., Zhou, L. (2016) Dry Reforming of Methane for Syngas Production Over Well-Dispersed Mesoporous NiCe0.5Zr0.5O3 with Ni Nanoparticles Immobilized. *Catal. Letters*, 146, 1663–1673, DOI: 10.1007/s10562-016-1791-9.

[48] Marinho, A.L.A., Rabelo-Neto, R.C., Epron, F., Toniolo, F.S., Noronha, F.B., Bion, N. (2022) Effect of Metal Dopant on the Performance of Ni@CeMeO2 Embedded Catalysts (Me = Gd, Sm and Zr) for Dry Reforming of Methane. *Methane*, 1, 300–319. DOI: 10.3390/methane1040023.

[49] Zhang, F., Liu, Z., Chen, X., Rui, N., Betancourt, L.E., Lin, L., Xu, W., Sun, C.J., Abeykoon, A.M.M., Rodriguez, J.A., et al. (2020) Effects of Zr Doping into Ceria for the Dry Reforming of Methane over Ni/CeZrO2 Catalysts: In Situ Studies with XRD, XAFS, and AP-XPS. *ACS Catal.*, 10, 3274–3284. DOI: 10.1021/acscatal.9b04451.